

Studies of the 2α and 3α channels of the $^{12}\text{C}+^{12}\text{C}$ reaction in the range of $E_{\text{c.m.}}=8.9$ MeV to 21 MeV using the active target Time Projection Chamber*

X. Y. Wang(王新雨)^{1,2,3,4} N. T. Zhang(张宁涛)^{2,4†} Z. C. Zhang(张志超)² C. G. Lu(鲁辰桂)^{2,4‡} T. L. Pu(蒲天磊)²
 J. L. Zhang(张金龙)^{2,3,4} L. M. Duan(段利敏)^{2,4} B. S. Gao(高丙水)^{2,4} K. A. Li(李阔昂)^{2,4} Y. T. Li(李宇田)^{2,4}
 Y. Qian(千奕)^{2,4} L. H. Ru(茹龙辉)^{2,4} B. Wang(王兵)² X. D. Xu(徐晓栋)^{2,4} H. Y. Zhao(赵红赟)^{2,4}
 W. P. Lin(林炜平)⁵ Z. W. Cai(蔡紫葳)⁶ B. F. Ji(姬彬斐)⁶ Q. T. Li(李奇特)⁶
 J. Y. Xu(许金艳)⁶ X. D. Tang(唐晓东)^{1,2,4}

¹Joint department for nuclear physics, Institute of Modern Physics and Lanzhou University, Chinese Academy of Sciences, Lanzhou 730000, China

²Institute of Modern Physics, Chinese Academy of Sciences, Lanzhou 730000, China

³School of Nuclear Science and Technology, Lanzhou University, Lanzhou 730000, China

⁴School of Nuclear Science and Technology, University of Chinese Academy of Sciences, Beijing 100049, China

⁵Key Laboratory of Radiation Physics and Technology of the Ministry of Education, Institute of Nuclear Science and Technology, Sichuan University, Chengdu 610064, China

⁶School of Physics and State Key Laboratory of Nuclear Physics and Technology, Peking University, Beijing 100871, China

Abstract: The $^{12}\text{C}+^{12}\text{C}$ fusion reaction was studied in the range of $E_{\text{c.m.}}=8.9$ to 21 MeV using the active-target Time Projection Chamber. With full information on all tracks of the reaction products, cross sections of the $^{12}\text{C}(^{12}\text{C},^8\text{Be})^{16}\text{O}_{\text{g.s.}}$ channel and the $^{12}\text{C}(^{12}\text{C},3\alpha)^{12}\text{C}$ channel could be measured down to the level of a few millibarns. The $^{12}\text{C}(^{12}\text{C},^8\text{Be})^{16}\text{O}_{\text{g.s.}}$ reaction channel was determined to be 10^{+24}_{-8} mb at $E_{\text{c.m.}}=11.1$ MeV, supporting the direct α transfer reaction mechanism. The $^{12}\text{C}(^{12}\text{C},3\alpha)^{12}\text{C}$ reaction channel was studied for the first time using an exclusive measurement. Our result does not confirm the anomaly behavior reported in the previous inclusive measurement by Kolata *et al.* [Phys. Rev. C **21**, 579 (1980)]. Our comparisons with statistical model calculations suggest that the 3α channel is dominated by the fusion evaporation process at $E_{\text{c.m.}} > 19$ MeV. The additional contribution of the 3α channel increases the fusion reaction cross section by 10% at energies above 20 MeV. We also find that an additional reaction mechanism is needed to explain the measured cross section at $E_{\text{c.m.}} < 15$ MeV at which point the statistical model prediction vanishes.

Keywords: fusion cross section, Coulomb barrier, Time Projection Chamber, active target

DOI: 10.1088/1674-1137/ac7a1d

I. INTRODUCTION

The $^{12}\text{C}+^{12}\text{C}$ fusion reaction at deep sub-barrier energies is a key reaction in massive stars, type Ia supernovae and superbursts [1–3]. Lacking sufficient detection sensitivity, direct measurements are currently limited to $E_{\text{c.m.}} > 2.1$ MeV. Theoretical extrapolation is indispensable for determining the reaction rate for astrophysical applications. The coupling effect of the excited states of projectile and target nuclei is important for the prediction of the fusion reaction cross section at energies around and below the Coulomb barrier. Esbensen *et al.*

[4] studied the coupling effect in the $^{12}\text{C}+^{12}\text{C}$ fusion reaction and pointed out that mutual excitations to the high-lying states of 2^+_1 at 4.44 MeV, 0^+_2 at 7.654 MeV and 3^-_1 at 9.641 MeV of ^{12}C play an important role. While the transition from the ground state to 2^+_1 is relatively well determined [5], the other transitions to the 0^+_2 and 3^-_1 states lack sufficient experimental constraints. As the 0^+_2 and 3^-_1 states decay via the 3α channel, a direct measurement of the inelastic scattering of $^{12}\text{C}(^{12}\text{C},3\alpha)^{12}\text{C}$ will provide a useful constraint for studies of fusion reactions around and below the Coulomb barrier. However, the measurement of the $^{12}\text{C}(^{12}\text{C},3\alpha)^{12}\text{C}$ channel is rather diffi-

Received 25 May 2022; Accepted 20 June 2022; Published online 16 August 2022

* Supported in part by the Strategic Priority Research Program of Chinese Academy of Sciences (XDB34020200), the National Key Research and Development program (MOST 2016YFA0400501) from the Ministry of Science and Technology of China, the State Key Laboratory of Nuclear Physics and Technology, PKU (NPT2020KFY06) and the National Natural Science Foundation of China (U1632142, 12175156), the National Natural Science Foundation of China (11905260) and the Western Light Project of Chinese Academy of Sciences

† E-mail: zhangningtao@impcas.ac.cn

‡ E-mail: luchengui@impcas.ac.cn

©2022 Chinese Physical Society and the Institute of High Energy Physics of the Chinese Academy of Sciences and the Institute of Modern Physics of the Chinese Academy of Sciences and IOP Publishing Ltd

cult as it involves a relatively high multiplicity and the difficult detection of low energy charged particles. There has been no direct measurement of the 3α channel to date. Kolata *et al.* determined the 3α cross section by subtracting the contributions of the α and 2α channels from the observed γ -ray yields [5, 6] from the summed α particle yield. However their result showed a minimum cross section at $E_{c.m.} \sim 19$ MeV. Such an abnormal behavior is difficult to explain using any theory. An exclusive measurement of $3\alpha+^{12}\text{C}$ is needed to verify the result.

The $^{12}\text{C}(^{12}\text{C}, ^8\text{Be})^{16}\text{O}$ channel is a possible channel for the $^{12}\text{C}+^{12}\text{C}$ fusion reaction. It was found that the ^8Be channel reaction cross section is smaller at $E_{c.m.} \geq 3.91$ MeV, but larger at $E_{c.m.} \leq 3.13$ MeV than the $\alpha_0+^{20}\text{Ne}_{g.s.}$ channel cross section. It was also found the cross section exceeds the DWBA calculation by nearly 3 orders of magnitude at $E_{c.m.}=2.43$ MeV, suggesting that the formation of $^{12}\text{C}+^{12}\text{C}$ dinuclear states becomes a predominant process at incident energies of $E_{c.m.} \leq 3.13$ MeV [7]. As the outgoing ^8Be decays into two α particles at low energies, the detection of this channel in the overwhelming background arising from elastic scattering processes is quite challenging. So far, this reaction channel has only been studied once at sub-barrier energies using an emulsion detector [7]. New experimental techniques are needed to push the measurement down to sub-barrier energies to further study the $^8\text{Be}+^{16}\text{O}$ reaction channel.

Fusion reactions involving weakly bound nuclei are important for nuclear physics as well for the development of the superburst model in astrophysics [1, 8]. However, such experiments are rare due to low radioactive ion beam intensities and a low detection efficiency. To overcome these difficulties, an active target method has been developed (see Refs. [9, 10] and references therein). The active target detector acts as the target for the reaction and as the detection medium at the same time. These detectors are usually designed in the form of a multi-sampling ionization chamber or Time Projection Chamber (TPC), which have nearly 4π solid angle coverage for charged particle detection [10, 11]. The incident particles and reaction products can be tracked by the detector, enabling the use of a thick target without inducing additional significant losses in energy resolution. The fusion excitation functions could be measured over a wide energy range using a single incident beam energy. For example, a MUSIC detector was used at the Argonne National Laboratory for measuring the cross sections of the $^{10,12-15}\text{C}+^{12}\text{C}$ systems with a beam intensity varying between 500 and 5000 particles/sec [12, 13]. The fusion cross section was determined by identifying the fusion evaporation residues against the elastic or inelastic scattering events based on their different ionization energy losses in the gas volume. Due to the absence of 3 dimensional (3D) tracks in MUSIC, accurate measurements of the reaction multiplicity and the stopping power of each

product cannot be obtained. A measurement of the fusion cross section below ~ 100 mb is rather challenging. A more complete measurement of the fusion residues and the decayed particles is needed to lower the limit of the cross section measurement.

We present the first experiment involving exclusive measurements of the excitation functions for the 3α channels of $^{12}\text{C}+^{12}\text{C}$ at energies around the Coulomb barrier. With the three dimensional tracking capability of TPC, the 2α , 3α particles and ^8Be channels could be detected in addition to the reaction residues. Although the beam intensity is only a few hundreds of counts per second (cps), the exclusive measurement of the 2α , 3α channels pushes the measured cross section limit down to 10 mb. Our measurement of the 3α channel contradicts the minimum cross section observed at $E_{c.m.}=19$ MeV. In the following sections, the detector setup and experimental procedure are described. The experimental results are presented together with a discussion of the results.

II. EXPERIMENTAL DETAILS

The experiment was performed with a 1024-channel TPC named pMATE (prototype Multi-purpose time projection chamber for nuclear Astrophysical and Exotic beam experiments). A schematic of the experimental setup and pMATE TPC detector are shown in Fig. 1. The primary beam of $^{12}\text{C}^{4+}$ was delivered from the sector-focusing cyclotron at the Heavy Ion Research Facility in Lanzhou (HIRFL), China [14]. The beam energy and beam current were 4.91 MeV/u and 300 enA, respectively. In order to obtain a low beam intensity down to the order of several 10^2 cps for the active target, the ^{12}C particle was scattered by a gold foil with a thickness of 0.81 mg/cm² in a scattering chamber. The TPC was installed at a scattering angle of 30° , as shown in Fig. 1. The scattered ^{12}C particle entered the TPC gas chamber through a 10 μm mylar foil with a 10-mm opening aper-

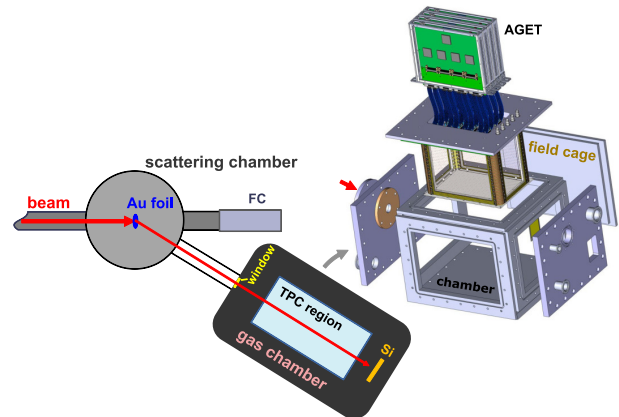


Fig. 1. (color online) Schematic of the experimental setup used for the measurement.

ture, which was 80 cm away from the scattering Au foil. pMATE TPC was mounted inside a 380 mm (L) \times 355 mm \times 285 mm (H) stainless chamber. In this $^{12}\text{C}+^{12}\text{C}$ measurement, isobutane (C_4H_{10}) was used as the active target. The gas pressure and flow were controlled by a gas handling system to ensure the stability of the TPC running conditions during the test and measurement. In order to cover a wide energy range of the reaction, the gas pressure in TPC was set to 106 mbar and 50 mbar. In the latter case, an aluminum degrader with a thickness of 29 μm was placed before the TPC entrance window for tuning the beam energy to the wanted energy range.

The pMATE TPC has an active volume of 100 mm \times 200 mm \times 200 mm (H). With a uniform electric field, which was formed by field wires, electrons from primary ionizations in the active region drift towards the anode readout plane. The avalanche of primary electrons, known as gas amplification, is performed using a stack of 2 thick Gaseous Electron Multipliers (GEMs) mounted on the readout plane [15]. In order to measure the multiplicity for reaction products, the anode is segmented into 32×32 rectangular pads of 3×6 mm², which is shown in the upper part of Fig. 2. The pad columns are numbered from 0 to 31 along the incident beam direction (z axis in Fig. 2). A detailed description of the pMATE TPC and its performance can be found in Ref. [16].

The pad signals are read out using a 1024-channel digitized GET system [17]. The trigger rate is limited to 500 Hz considering the number of fired pads to be around 90 for each event. The corresponding data flow rate is estimated to be on the order of ~ 100 MB/s. In order to reduce the data flow and the possible data loss, it is necessary to avoid triggering the unreacted beam ions and elastic events at forward angles. For this purpose, a silicon detector was installed downstream of the TPC field cage inside the gas chamber (see Fig. 1). In the $^{12}\text{C}+^{12}\text{C}$ fusion reaction, the heavy residues tend to travel in a direction close to the incident beam. The gas pressure was adjusted to ensure the fusion residues stopped before the Si detector, while the unreacted beam particles could be detected by the Si detector. An anticoincidence between the signal from the Si detector and the signal from the GEM of TPC was used as the trigger for the GET electronics for capturing fusion reaction events and removing unreacted beam particles and most of the forward scattering events. To obtain the beam particle profile in TPC, the signal of the Si detector was also used occasionally in some runs after being scaled down.

In the current experimental setup, a constant gain optimized for fusion-residue and α particle detection is achieved over the entire pad plane. The detection threshold is around 50 keV in each readout pad. Alpha particles with energies above ~ 15 MeV or protons with energies above ~ 0.56 MeV do not generate tracks in TPC as their energy depositions in each pad are below the de-

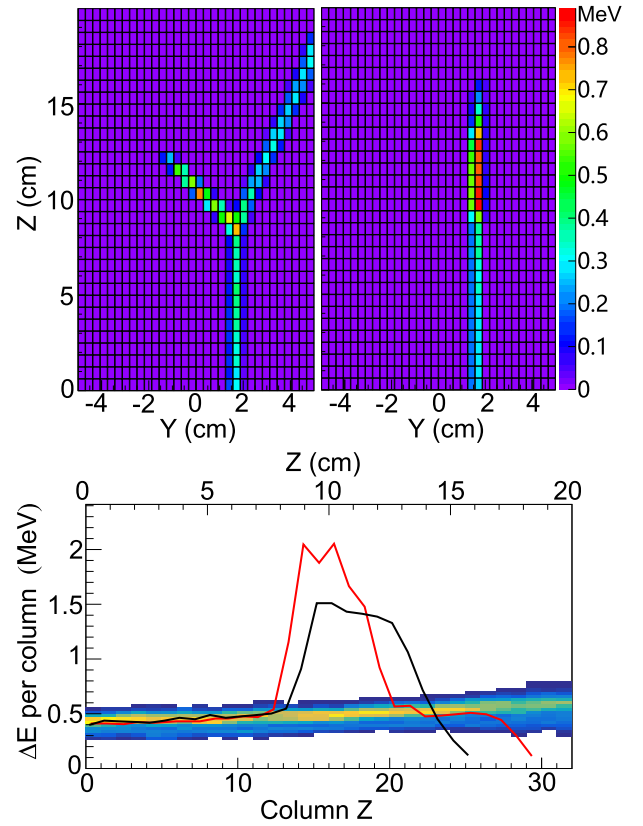


Fig. 2. (color online) Events measured with the pMATE TPC at a gas pressure of 50 mbar. (top) Trajectories projected in the readout pad plane for one typical scattering event (left) and fusion event (right). The color is proportional to the energy-loss on each pad. (bottom) Histogram of the energy-loss profile of the unreacted beam particles along their incident direction. The energy-loss profiles of the reaction events in the top panel (red line \rightarrow top left, black line \rightarrow top right) are also plotted for comparison. The pad columns are numbered from 0 to 31 along the z axis, which defines the beam direction.

tection threshold.

III. ANALYSIS AND DISCUSSION

A. Track reconstruction

One advantage of the active-target TPC is that it records the tracks of every charged particle and provides the energy-loss, position and angle for each track. This capability cannot only help us tune the beam direction and reject events coming from scattering on the entrance window foil or the wires of the field cage, but is also crucial for an unambiguous identification of the type of reaction. The experimental traces of a typical scattering event and a fusion event measured with pMATE TPC are shown in Fig. 2. On the bottom of Fig. 2, the Bragg curves (energy-loss in each pad column along the beam incident direction) of these two events are shown togeth-

er with the energy-loss profiles of the unreacted beam particles passing through the TPC gas region. The Bragg curves for these reaction events are similar to the energy-loss signals of beam particles before the reaction happens. When the reaction happens, the Bragg curve suddenly increases around the reaction vertex. As shown in Fig. 2, it is rather challenging to cleanly identify fusion events based only on these interfering elastic or inelastic scattering events. Information on the tracks of the emitted light particles from the fusion reaction is needed to determine the exact type of reaction.

Identification of the trajectories of the reaction products is the major task in a reconstruction of the reaction events. For most nuclear reaction measurements using TPC, the light particles from the reactions are usually scattered at large angles relative to the projectiles. In these cases, track reconstruction is straightforward. By extrapolating the tracks to the beam axis, the reaction vertex can be determined. In the case of fusion studies, reconstruction is complicated by the fact that the direction of the fusion residues is close to the beam direction. In order to eliminate interference from beam ions, the beam trajectory before the reaction has to be removed first. In our analysis, a pad region is defined for the ^{12}C beam according to the beam trajectory projected on the pad plane. Using the energy-loss (ΔE) profile in this beam region, as shown in Fig. 2, the reaction position (or column) can be determined by checking ΔE . The fired pads from this position to the beam entrance correspond to the beam trajectory and are removed from further track analyses of the reaction products.

An example of a track reconstruction for one elastic/inelastic scattering event obtained in our experiment is shown in Fig. 3. Two scattering particles cannot be separated at the point at which the two tracks merge in the readout pad plane (top panel in Fig. 3). However, in the drift plane, which is perpendicular to the readout plane, two distinct tracks are observed, as shown in the middle panel of Fig. 3. The drift coordinate is determined by the electron drift time multiplied by the drift velocity. Here, we adopted the two-dimensional Hough transform method for separating the track, an algorithm commonly used in image analysis based on a given set of image pixels (see Ref. [18]). In the Hough transformation, each point at (x, y) is transformed into a curve in the (θ, R) parameter space (Hough space) using the formula $R = x \cos \theta + y \sin \theta$ in the θ interval of $0 \leq \theta \leq \pi$. If the pixels in the pad or drift plane form a straight line, their transformed curves will intersect at one point in Hough space. As an example, the points in the drift plane (middle panel in Fig. 3) are transformed into the Hough space shown at the bottom of Fig. 3. It should be noted that the points of the unreacted beams were removed before the transformation. By searching the intersection points in the Hough space in an iterative way, multiple tracks were de-

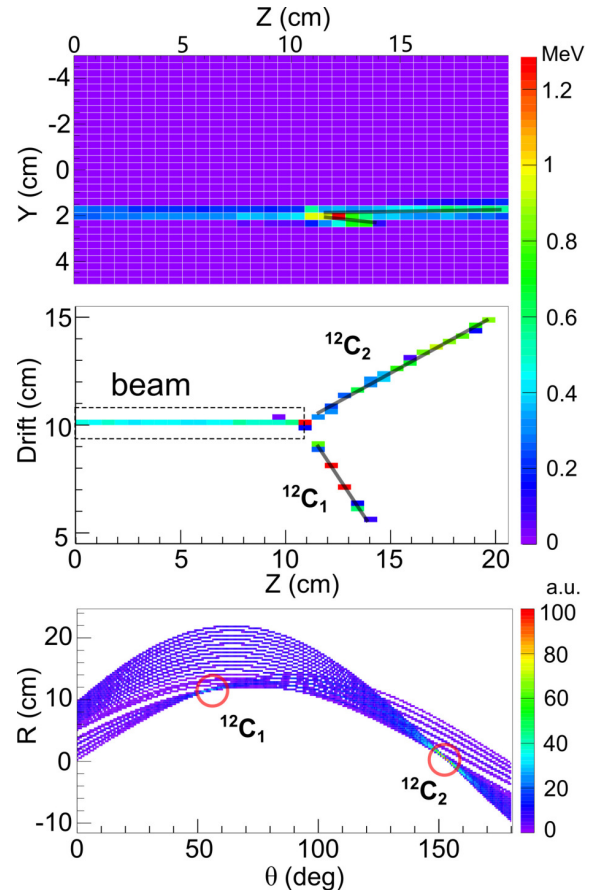


Fig. 3. (color online) Example of a $^{12}\text{C}+^{12}\text{C}$ scattering event. (top) Track projection to the pad plane. (middle) Projection to the drift plane along the electron drift direction. The solid lines are the linear fittings of the tracks identified by the Hough transform algorithm. (bottom) Hough space made from the points in the middle panel, where the points belonging to the beam were removed before the transformation. The red open circles indicate identified particle trajectories.

termined separately. The solid straight lines in this figure represent the linear fittings, which are weighted by the charges deposited on each pad. It is seen that this procedure shows a good and stable track reconstruction performance over the entire range for scattering particles. Using 3D tracks, the particle energy loss, range and angle can be obtained and the reaction vertex can be calculated by tracing back to the beam axis.

The response of the pMATE TPC to the fusion reaction was also investigated using a similar tracking method. The top plot of Fig. 4 shows a strong ionization at the end of the beam-like trajectory. Looking at the event trajectories in the drift plane at the bottom of Fig. 4, this track was identified to be formed by fusion residue which has higher A and Z than the ^{12}C beam. These particles are stopped quickly by the gas after the reaction. The energy loss of another track is very different. The ΔE per pad is about ten times smaller than that of the ^{12}C beam. As the

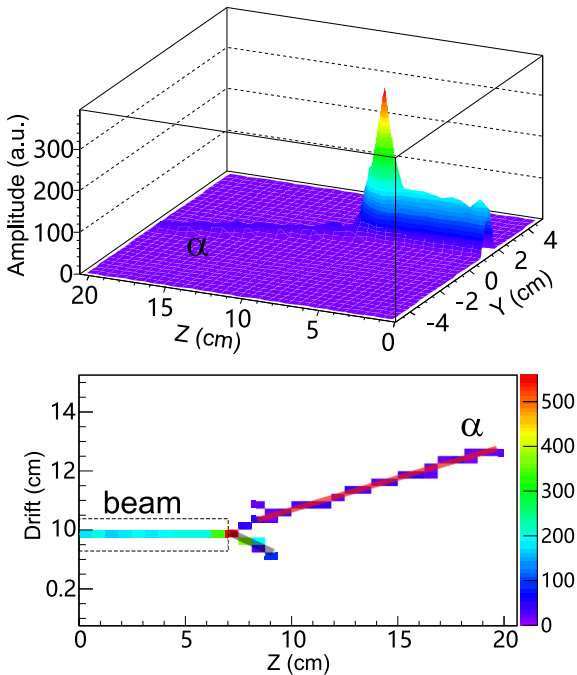


Fig. 4. (color online) Energy-loss for a fusion event with one α emission. (top) Projection of the energy-loss in the pad plane. (bottom) Track projection in the drift plane. The straight lines are the linear fittings of the tracks identified by the Hough transform algorithm.

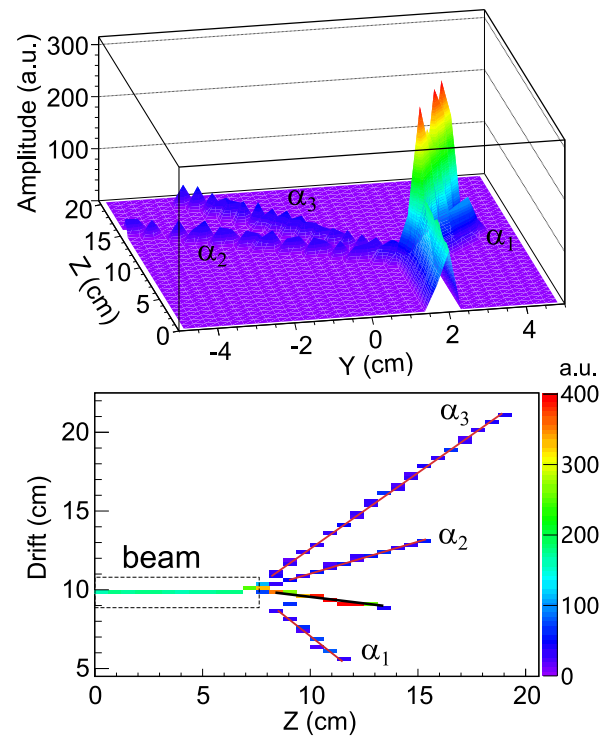


Fig. 5. (color online) Similar to Fig. 4, but for 3α emission from a $^{12}\text{C}+^{12}\text{C}$ reaction event.

proton is below the detection threshold and no tritons or ^3He are expected in the $^{12}\text{C}+^{12}\text{C}$ reaction in the current energy range, we can identify this particle as being an alpha using its energy-loss profile in the gas. Note that the range of the fusion residue in the gas is relative short and hence its points in Hough space sometimes fall into the alpha track. In order to resolve the track of heavy residue, we follow the changes in stopping power (dE/dX) along the 3D track. Starting from the end point in a track, the averaged dE/dX is calculated at each point with a step size of 12 mm towards the reaction vertex. If the averaged dE/dX becomes two times larger than the previous one, the corresponding data points after that position will be removed from the track. These filtered points will be analyzed by a new Hough transform to identify the alpha track.

An example of a four body event in the exit channel is shown in Fig. 5. Due to the good tracking capability for multiple tracks, three evaporated alpha particles were detected directly and the recoiling fusion residue is also clearly seen here. After removing the beam trajectory, all recorded trajectories were reconstructed successfully using Hough transformation, as shown in Fig. 5.

The emission of a heavier cluster decay $^{12}\text{C}+^{12}\text{C} \rightarrow ^{16}\text{O}+^8\text{Be}$ (g.s.) has been studied extensively in previous works [7, 19, 20]. It was also observed in this work. For a ground-state ^8Be decay, two alpha particles are emitted with a narrow opening angle between each other. An ex-

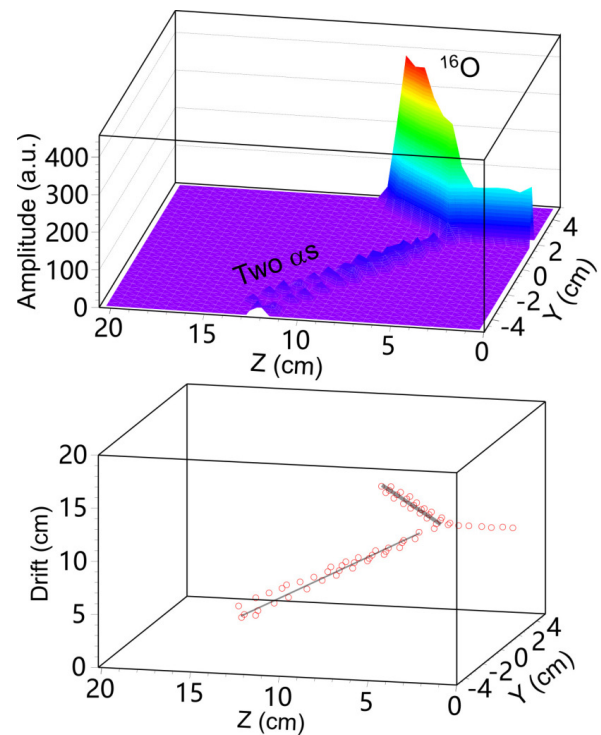


Fig. 6. (color online) Energy-loss plot for a fusion event with a possible ^8Be -particle emission. (top) Projection of the energy-loss in the pad plane. (bottom) Three dimensional points for track reconstruction. The straight lines are the linear fittings of the tracks identified by the Hough transform algorithm.

ample, as observed in this work is shown in Fig. 6.

B. $^{12}\text{C}+^{12}\text{C}$ fusion cross section

To identify the $^{12}\text{C}+^{12}\text{C}$ fusion events, the maximum stopping power (dE/dX_{max}) of each track is calculated using a step size of 1 cm. In Fig. 7(a), dE/dX_{max} is plotted against the total ionization energies of the tracks for different particles. In this plot, alpha particles from the fusion events are located around the coordinate origin and can be clearly separated from the scattering events. Fusion residues with a recoil energy of more than 5 MeV are also well separated from the scattering events. However, some residues with smaller energies have rather smaller dE/dX_{max} and partly overlap with the scattered particles.

For reaction channels evaporating protons and neutrons (xpn channels), the kinematic kick on the fusion residue is less significant than for channels which include the evaporation of α particle(s). dE/dX_{max} versus the kinetic energy spectrum of the fusion residues is shown in Fig. 7(b). In the current experiment, the kinetic energies of the fusion residues were high enough to be separated from the beam particle, ^{12}C . For the $\alpha(s)+xpn$ channels, once an alpha particle is identified, this reaction can be categorized as a fusion event. The dE/dX_{max} spectra gated with detection of 1 α and ≥ 2 α s are shown in Figs. 7(c) and (d), respectively. Due to the requirement of an α track, the fusion residues can be well identified without any interfering scattering events.

The fusion reaction yields are obtained by counting the number of fusion events in each pad column along the beam direction. As the first and last several columns were required to detect the tracks of beam and reaction particles, the current pMATE TPC provided 18–20 energy points in each run. The number of ^{12}C beam particles was determined from the rates recorded by Silicon downstream. A realistic Geant4 simulation was performed to determine the beam energy at each reaction vertex and the energy uncertainty. In the current work, uncertainty in the reaction energies was determined (e.g. ~ 0.84 MeV (1σ) at $E_{\text{beam}}=22$ MeV), which is dominated by the kinematic broadening of the scattered ^{12}C s by the Au target and energy straggling in the degrader and the counting gas.

The fusion cross sections were obtained in the ranges of $E_{\text{c.m.}}=15.3\text{--}21.1$ MeV and $E_{\text{c.m.}}=8.93\text{--}13.69$ MeV with gas pressures of 106 and 50 mbar, respectively. Due to false triggers in the GET system during the measurement at 50 mbar, we were not able to determine the absolute cross section of the $^{12}\text{C}+^{12}\text{C}$ reaction. To solve this problem, the total fusion cross sections in the second run at 50 mbar are normalized to the results measured by Kovar *et al.* [21] with a scaling factor determined with a chi-square analysis. The total fusion cross sections shown in Fig. 8 agree well with the previous measurement [21] and the

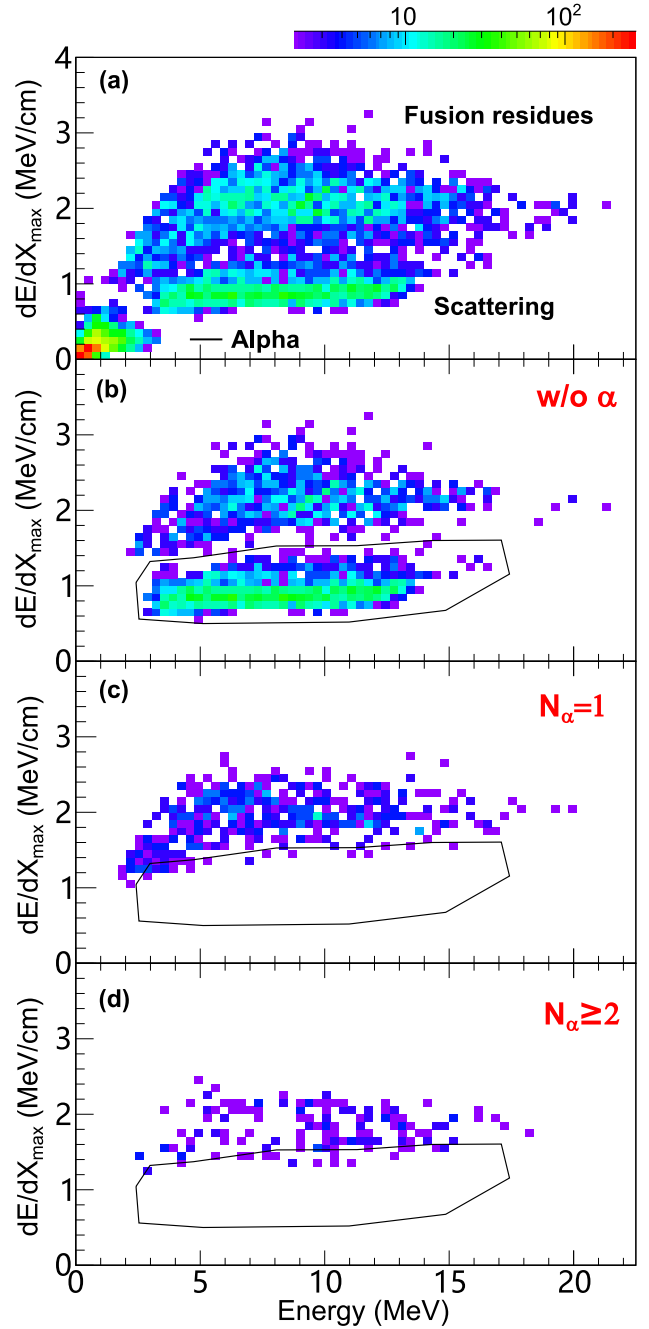


Fig. 7. (color online) dE/dX_{max} versus total energy deposition of particle (E) for the detected particles in TPC. The data were obtained at a pressure of 50 mbar and the plots were generated under the following conditions: (a) all tracks of the reaction products, (b) no alpha tracks identified in the reaction products, (c) single alpha particle identified in the reaction products, and (d) two or more alpha particles identified in the reaction products. Events localized around the coordinate origin come from the alpha particles. Regarding fusion residues with a recoil energy of less than 5 MeV, they partly overlap with the scattered particles indicated with a black polygon. By requiring the presence of α particles, the fusion residues can be clearly identified without interference by the scattering events.

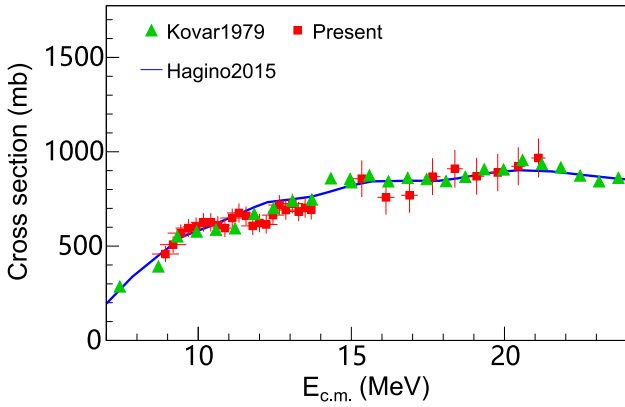


Fig. 8. (color online) Measured excitation function of the total fusion cross section (red solid squares). Data from Ref. [21] and theoretical calculations [23] are plotted for comparison and shown respectively as triangles and a blue solid line.

calculations using the the energy-dependent version of Wong's formula proposed by Rowley and Hagino [22].

C. $^{12}\text{C}(^{12}\text{C},2\alpha)^{16}\text{O}$ channel

The dominant channel of the $2\alpha + xpn$ channels is $^{12}\text{C}(^{12}\text{C},2\alpha)^{16}\text{O}$, as the other channels are negligibly small according to the statistical model calculation using Empire [24]. For example, the cross section ratio of $^{12}\text{C}(^{12}\text{C},2\alpha+p)^{15}\text{N}$ to $^{12}\text{C}(^{12}\text{C},2\alpha)^{16}\text{O}$ is estimated to be 0.02 according to Empire. The contributions of the other channels are even smaller or totally closed due to the energy threshold.

The 3-body decay events were simulated in the 2α sequential decay mode. TGenphasespace provided by ROOT [25, 26] was used to generate the phasespaces of these decay particles. The population and decay probabilities of the excited states in the intermediate ^{20}Ne nucleus were taken from the statistical model calculation. In the ^8Be mode, an ^8Be particle is emitted before it decays into two α particles with a decay energy of 93 keV.

The 2α sequential decay was simulated using the statistical model codes, Empire and Talys [27]. The population of the excitation energy distribution of the ^{16}O is shown in Fig. 9. Using the kinetic energy derived from the measured range and angle of the detected ^{16}O , the Q value was calculated using the following equation,

$$Q = \left(\frac{12}{8} - 1\right)E_1 + \left(\frac{16}{8} + 1\right)E_3 - 2\frac{\sqrt{12 \cdot 16 \cdot E_1 \cdot E_3}}{8} \cos\theta_3. \quad (1)$$

Here E_1 is the beam energy in the laboratory frame, E_3 is the kinetic energy of ^{16}O as derived from the measured range in TPC, and θ_3 is the angle of ^{16}O . The spectrum of the Q value is shown in Fig. 10. It should be noted that the Q value includes not only the excitation energy of ^{16}O but also the internal kinetic energy of the two α particles

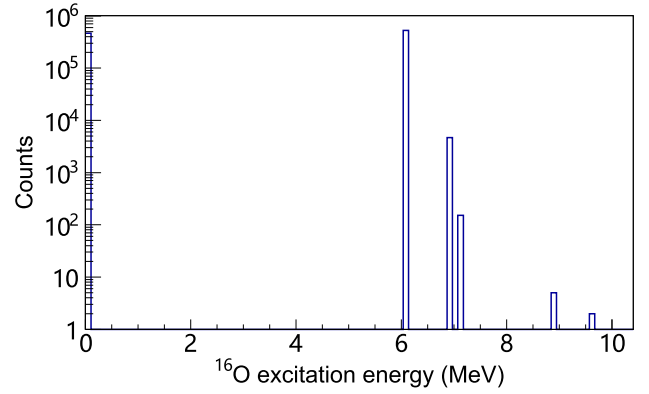


Fig. 9. (color online) Excitation energy spectrum of ^{16}O simulated using the statistical model at $E_1=24$ MeV.

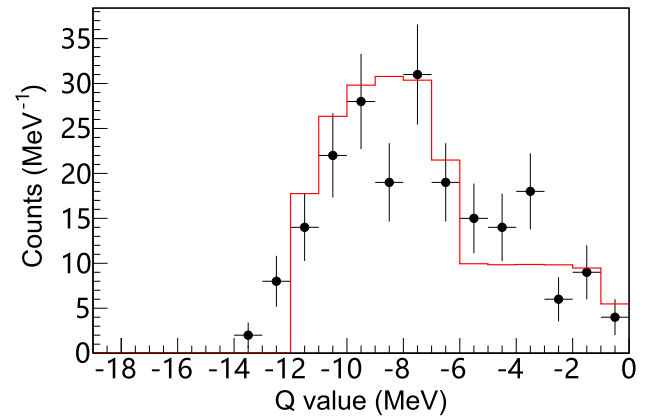


Fig. 10. (color online) Experimental Q -value spectrum calculated with the kinetic energy and angle of ^{16}O for events in the range of $E_1=18-28$ MeV. The red line is the simulated result with $E_1=24$ MeV.

in the center of mass frame (CM) of the two α particles. The minimum internal kinetic energy of the two α particles is 0 while the maximum value corresponds to the zero kinetic energy of ^{16}O in the CM frame, which can be calculated using $E_1/2 + Q_0 - E_x$. Here E_x is the excitation energy of ^{16}O and Q_0 equals -0.113 MeV, which is the Q value of the channel decaying to the ground state of ^{16}O . The allowed Q -value range for ^{16}O for a given E_x is from $-E_x - 0.113$ MeV to $-E_1/2 - 0.113$ MeV. According to the statistical model prediction at $E_1=24$ MeV shown in Fig. 9, the most populated states of ^{16}O are the ground state and the excited state at 6.049 MeV. Therefore, the Q values of the ground state and the 6.049 MeV state range from -0.113 to -12 MeV and from -6.162 to -12 MeV, respectively. Our experimental result shown in Fig. 10 confirm these results.

Simulations of ^{16}O ($\theta_{16\text{O}}$) angle versus the opening angle between two α particles ($\theta_{2\alpha}$) are shown together with the experimental results in Fig. 11. It is clear that the majority of the experimental results agrees well with the simulation result using the statistical model calculation.

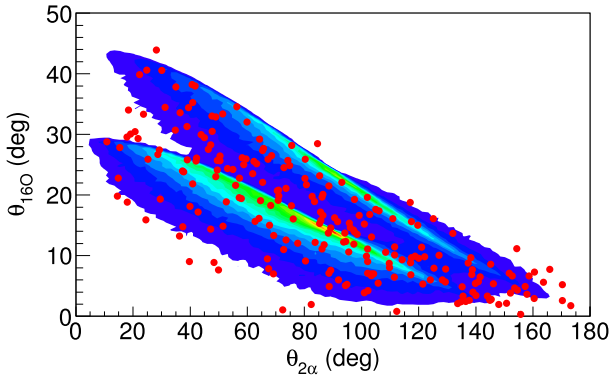


Fig. 11. (color online) Spectrum of the angle of ^{16}O ($\theta_{16\text{O}}$) versus the opening angle between the two α particles. Data points are obtained from the measurement at 50 mbar. The simulation done in the 2α sequential decay mode and the experimental results are shown in contour and scattered points, respectively. The contours cover 95% of the total simulated events.

D. $^{12}\text{C}(^{12}\text{C}, ^8\text{Be})^{16}\text{O}$ channel

It is also possible that two α particles are emitted together as a ^8Be which decays into 2α particles. The traditional approach is to measure the energies and angles of the two emitting α s and then identify the ^8Be cluster with the reconstructed relative kinetic energies of the 2α s [20]. Identification of ^8Be has also been reported simply based on the measurement of the polar angle between the two α particles [19] in the range from $E_{\text{c.m.}}=17.5$ to 34.5 MeV. The active target captures both ^{16}O and the two α particles with a 100% geometric efficiency with a nearly complete kinematic measurement. The only missing information is the energies of the two α particles which penetrate the active volume in the current experiment.

The simulated spectra of the ^{16}O angle versus the opening angle between the two α s using the ^8Be emission mode are shown together with the experimental results in Fig. 12. The states of the final residue, $^{16}\text{O}^*$, include the ground state and the excited states at 6.049, 6.13, 6.917, 7.116 and 8.872 MeV. States with higher excitation are not included because they decay by alpha emission. To investigate the contributions of different ^{16}O states, the spectrum is generated by gating the Q value obtained with the detected range and the angle of ^{16}O . In total, we find 1 event that agrees with the simulation done using the ground state of ^{16}O , corresponding to 10_{-8}^{+24} mb.

Our result is shown together with the cross section measurement by Čujec *et al.* [7] as the modified S factor ($S^* = \sigma \cdot E \cdot \exp(87.21/\sqrt{E} + 0.46E)$) in Fig. 13. Considering $^{12}\text{C}(^{12}\text{C}, ^8\text{Be})^{16}\text{O}_{\text{g.s.}}$ a direct α -transfer reaction, the cross section has been evaluated for the $L=0$ transfer in the distorted-wave Born approximation (DWBA) with the PTOLEMY program [28]. The optical-model potential ($V=-50$ MeV, $W=-10$ MeV, $R_0 = 1.26$ fm, and $a=0.4$ fm) is used in the DWBA calculation for ingoing and outgo-

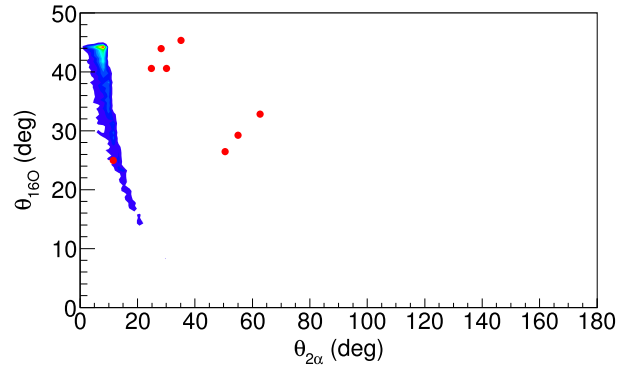


Fig. 12. (color online) Spectrum of the angle of ^{16}O ($\theta_{16\text{O}}$) vs. the opening angle between the two α particles from ^8Be emission. The simulated and experimental results measured at 50 mbar are shown in contours and scattered points, respectively. A cut of $\text{abs}(Q\text{-value}) < 1$ MeV is applied to the experimental data.

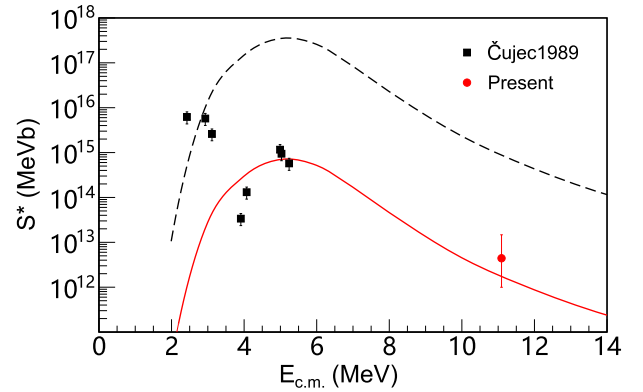


Fig. 13. (color online) Modified S factor (S^*) of $^{12}\text{C}(^{12}\text{C}, ^8\text{Be})^{16}\text{O}_{\text{g.s.}}$. Current measurements and those of Čujec are shown as red and black points, respectively. The red solid and black dashed lines are the DWBA calculations using the product of spectroscopic factors of 0.06 and 30, respectively.

ing channels, which is taken from Ref. [7]. In the calculation, the node number of the α -cluster was set to 2 according to the shell model configuration. The product of the alpha spectroscopic factor was set to 0.03 according to the theoretical calculation [29]. Taking into account the identical nuclei in the entrance channel, an additional factor of 2 was applied to the calculated cross section to reproduce the calculation by Čujec *et al.* at energies around 5.5 MeV. In order to match with the experimental result at 2.93 MeV, the product of the spectroscopic factors needs to be scaled up by a factor of 500. However, our measurement agrees with the calculation using spectroscopic factors of 0.06, suggesting that $^{12}\text{C}(^{12}\text{C}, ^8\text{Be})^{16}\text{O}_{\text{g.s.}}$ is dominated by the direct α transfer process in the range of 3.13 to 12 MeV. The large difference between the experimental data and the DWBA calculation at lower energies indicates the possibility of new physics, e.g., the impact of the molecular structure in the

entrance channel on the reaction mechanism. While the emulsion detection used in the Čujec experiment is unable to record the coincidence of two α particles in the time domain, TPC can detect ^8Be unambiguously by recording the full information with the large background of scattered ^{12}C particles. Therefore, this offers a new opportunity for investigating the interesting channel below 3.13 MeV and helping us achieve a better understanding of the formation of ^8Be clusters in the $^{12}\text{C}+^{12}\text{C}$ reaction.

E. $^{12}\text{C}(^{12}\text{C},3\alpha)^{12}\text{C}$ channel

The complicated 3α channel can be easily identified against other contaminants by visualizing the α tracks together with the fusion residues in TPC. Our result is presented in Fig. 14. At energies above $E_{\text{c.m.}}=19$ MeV, our result tends to agree with the result of Kolata *et al.* [21]. Both measurements are consistent with the Empire calculation and support the explanation of fusion evaporation. Although the cross section of this channel is at the level of 100 mb at energies above 20 MeV, which is about 10% of the total fusion cross section, it has been ignored in the $^{12}\text{C}+^{12}\text{C}$ total fusion due to the technical challenge involved [21, 30]. Our measurement provides valuable data for the complete fusion cross section and our statistical model calculation proves the dominant contribution to be from the fusion evaporation reaction.

At energies below $E_{\text{c.m.}}=19$ MeV, the abnormal trend reported in Ref. [6] is replaced by much lower 3α cross

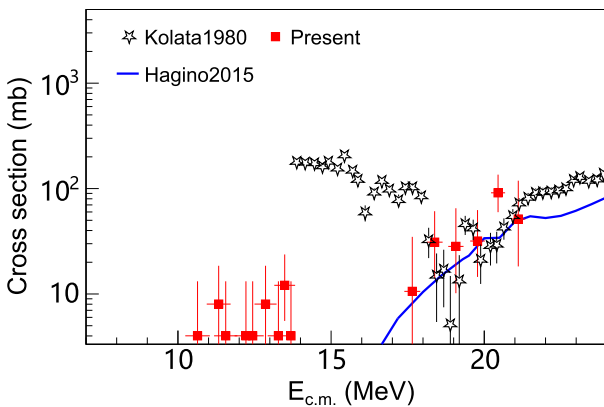


Fig. 14. (color online) Comparison of experimental 3α -emission cross sections with the statistical calculation. Red squares: experimental data obtained with pMATE TPC. Black stars: experimental data measured by Kolata *et al.* [5]. Blue line: Prediction of the fusion evaporation model calculated using EMPIRE. The total fusion cross section by EMPIRE is normalized to the calculation in Ref. [23].

sections and the localized minimum near 19 MeV disappears. At $E_{\text{c.m.}} < 15$ MeV, we still find some 3α events with a cross section at the level of 10 mb while the Empire calculation predicts a vanishing cross section. Considering that the cross section of inelastic scattering up to

the 4.44 MeV of ^{12}C is in the order of 100 mb around 15 MeV [5], the 3α events may indicate the possible contribution of a direct reaction other than fusion evaporation, such as the proposed inelastic scattering leading to $0^+(7.654$ MeV) and $3^-(9.641$ MeV) [4]. As the statistics of the current measurement are rather low and the kinetic energies of the α particles are missing, a follow-up measurement with better statistics will be useful in reconstructing the unbound states of the break-up 3α events, providing decisive evidence for the direct reaction component.

IV. SUMMARY AND OUTLOOK

The $^{12}\text{C}+^{12}\text{C}$ fusion reaction was studied in the range of $E_{\text{c.m.}}=8.9$ to 21 MeV using the active-target Time Projection Chamber. Due to full information on all tracks of the reaction products, the cross sections of the $^{12}\text{C}(^{12}\text{C},^8\text{Be})^{16}\text{O}_{\text{g.s.}}$ channel and the $^{12}\text{C}(^{12}\text{C},3\alpha)^{12}\text{C}$ channel were measured down to ~ 10 mb. The $^{12}\text{C}(^{12}\text{C},^8\text{Be})^{16}\text{O}$ reaction channel is determined to be 10^{+24}_{-8} mb at $E_{\text{c.m.}}=11.1$ MeV, supporting the direct α transfer reaction mechanism. The $^{12}\text{C}(^{12}\text{C},3\alpha)^{12}\text{C}$ reaction channel was studied for the first time using an exclusive measurement. Our measurement does not confirm the anomaly behavior reported in the previous inclusive measurement. Our comparisons with the statistical model calculations suggest that the 3α channel is dominated by the fusion evaporation process at $E_{\text{c.m.}} > 19$ MeV. The additional contribution of the 3α channel increases the fusion reaction cross section by 10% at energies above 20 MeV. We also find that an additional reaction mechanism is needed to explain the measured cross section at $E_{\text{c.m.}} < 15$ MeV at which point the statistical model prediction vanishes.

The techniques developed in this work provide a new opportunity for studying difficult reactions such as $^{12}\text{C}(^{12}\text{C},^8\text{Be})^{16}\text{O}_{\text{g.s.}}$ at $E_{\text{c.m.}} < 3$ MeV and fusion reactions involving radioactive ion beams. Compared with traditional detectors and techniques in nuclear physics, the main advantage of the pMATE TPC detector is the extremely high efficiency and its capability of simultaneous detection of multiple charged particles. In the active-target mode, reaction cross sections can be measured over a wide energy range down to a few millibarn with a beam intensity of ~ 100 particles per second. Motivated by this unique opportunity provided by TPC, fusion reactions induced by neutron-rich isotopes will be started in the future, which is very difficult using traditional detectors due to their low-intensity radioactive beams.

ACKNOWLEDGMENTS

The authors thank the HIRFL operation staff for providing beams during the experiment.

References

- [1] L. R. Gasques, E. F. Brown, A. Chieffi *et al.*, *Phys. Rev. C* **76**, 035802 (2007)
- [2] B. B. Back, H. Esbensen, C. L. Jiang *et al.*, *Rev. Mod. Phys.* **86**, 317-360 (2014)
- [3] Xiaodong Tang and Longhui Ru, *EPJ Web Conf.* **260**, 01002 (2022)
- [4] H. Esbensen, X. Tang, and C. L. Jiang, *Phys. Rev. C* **84**, 064613 (2011)
- [5] J. J. Kolata, R. M. Freeman, and F. Haas, *Haas, Phys. Rev. C* **21**, 579-587 (1980)
- [6] J. J. Kolata, R. E. Malmin, P. A. DeYoung *et al.*, *Phys. Rev. C* **21**, 776-778 (1980)
- [7] B. Čujec, I. Hunyadi, and I. M. Szöghy, *Phys. Rev. C* **39**, 1326-1334 (1989)
- [8] M. Beard, A. V. Afanasjev, L. C. Chamon *et al.*, *Atomic Data and Nuclear Data Tables* **96** (5) (2010) 541–566. URL <http://www.sciencedirect.com/science/article/pii/S0092640X10000331>
- [9] S. Beceiro-Novo, T. Ahn, D. Bazin *et al.*, *Progress in Particle and Nuclear Physics* **84**, 124-165 (2015)
- [10] L. F. Canto, V. Guimarães, J. Lubián *et al.*, *Eur. Phys. J. A* **56**(11), 281 (2020)
- [11] D. Bazin, T. Ahn, Y. Ayyad *et al.*, *Progress in Particle and Nuclear Physics* (2020) 103790. URL <http://www.sciencedirect.com/science/article/pii/S0146641020300375>
- [12] P. F. F. Carnelli, S. Almaraz-Calderon, K. E. Rehm *et al.*, *Phys. Rev. Lett.* **112**, 192701 (2012)
- [13] P. Carnelli, S. Almaraz-Calderon, K. Rehm *et al.*, *Nuclear Instruments and Methods in Physics Research Section A: Accelerators, Spectrometers, Detectors and Associated Equipment* **799**, 197-202 (2015)
- [14] W. Zhan, H. Xu, Z. Sun *et al.*, *International Journal of Modern Physics E* **15**, 1941-1956 (2006)
- [15] Q. Liu, H. B. Liu, S. Chen *et al.*, *Journal of Instrumentation* **8**(11), C11008 (2013)
- [16] Z. C. Zhang, X. Y. Wang, T. L. Pu *et al.*, *Nuclear Instruments and Methods in Physics Research Section A: Accelerators, Spectrometers, Detectors and Associated Equipment* **1016**, 165740 (2021)
- [17] J. Giovinazzo, T. Goigoux, S. Anvar *et al.*, *Nuclear Instruments and Methods in Physics Research Section A: Accelerators, Spectrometers, Detectors and Associated Equipment* **840**, 15-27 (2016)
- [18] R. O. Duda and P. E. Hart, *Commun. ACM* **15**(1), 11-15 (1972)
- [19] A. Weidinger, K. A. Eberhard, and E. Mathiak, *Nucl. Phys. A* **257**(1), 144-164 (1976)
- [20] N. R. Fletcher, J. D. Fox, G. J. KeKelis *et al.*, *Phys. Rev. C* **13**, 1173-1179 (1976)
- [21] D. G. Kovar, D. F. Geesaman, T. H. Braid *et al.*, *Phys. Rev. C* **20**, 1305-1331 (1979)
- [22] N. Rowley and K. Hagino, *Phys. Rev. C* **91**, 044617 (2015)
- [23] K. Hagino and J. M. Yao, *EPJ Web of Conferences* 117 (2016). URL <https://doi.org/10.1051/epjconf/201611708003>
- [24] M. Herman, R. Capote, B. V. Carlson *et al.*, *Nucl. Data Sheets* **108**(12), 2655-2715 (2007)
- [25] R. Brun and F. Rademakers, *Nuclear Instruments and Methods in Physics Research Section A: Accelerators, Spectrometers, Detectors and Associated Equipment* **389**(1), 81-86 (1997)
- [26] F. E. James, Monte Carlo phase space, CERN, Geneva, 1968, p. 41 p, CERN, Geneva, 1 May 1968 URL <https://cds.cern.ch/record/275743>
- [27] A. J. Koning and D. Rochman, *Nucl. Data Sheets* **113**(12, SI), 2841-2934 (2012)
- [28] D. H. Gloeckner, M. H. Macfarlane, and S. C. Pieper, Ptolemy, a program for heavy-ion direction-reaction calculations.[cross sections, optical model, dwba] (3 1976). URL <https://www.osti.gov/biblio/7363080>
- [29] M. Ichimura, A. Arima, E. C. Halbert *et al.*, *Nuclear Physics A* **204**(2), 225-278 (1973)
- [30] M. Conjeaud, S. Gary, S. Harar *et al.*, *Nuclear Physics A* **309**(3), 515-532 (1978)